The Folding Pathway of Barnase: The Rate-Limiting Transition State and a Hidden Intermediate under Native Conditions

Ngoc-Diep Vu, Hanqiao Feng, and Yawen Bai*

Laboratory of Biochemistry, National Cancer Institute, NIH, Building 37, Room 6114E, Bethesda, Maryland 20892

Received December 11, 2003; Revised Manuscript Received January 25, 2004

ABSTRACT: The nature of the rate-limiting transition state at zero denaturant (TS_1) and whether there are hidden intermediates are the two major unsolved problems in defining the folding pathway of barnase. In earlier studies, it was shown that TS_1 has small ϕ values throughout the structure of the protein, suggesting that the transition state has either a defined partially folded secondary structure with all side chains significantly exposed or numerous different partially unfolded structures with similar stability. To distinguish the two possibilities, we studied the effect of Gly mutations on the folding rate of barnase to investigate the secondary structure formation in the transition state. Two mutations in the same region of a β-strand decreased the folding rate by 20- and 50-fold, respectively, suggesting that the secondary structures in this region are dominantly formed in the rate-limiting transition state. We also performed native-state hydrogen exchange experiments on barnase at pD 5.0 and 25 °C and identified a partially unfolded state. The structure of the intermediate was investigated using protein engineering and NMR. The results suggest that the intermediate has an omega loop unfolded. This intermediate is more folded than the rate-limiting transition state previously characterized at high denaturant concentrations (TS_2). Therefore, it exists after TS_2 in folding. Consistent with this conclusion, the intermediate folds with the same rate and denaturant dependence as the wild-type protein, but unfolds faster with less dependence on the denaturant concentration. These and other results in the literature suggest that barnase folds through partially unfolded intermediates that exist after the rate-limiting step. Such folding behavior is similar to those of cytochrome *c* and Rd-apocyt b_{562}. Together, we suggest that other small apparently two-state proteins may also fold through hidden intermediates.

Folding of a small protein with ∼100 amino acids by random, unbiased searching for the native state cannot occur because it would take an infinite amount of time; yet it can reach to the native state within seconds. This large-scale conformational search problem, commonly phrased as the Levithal paradox (*1*) has been the major focus in the studies of protein folding for the past 30 years. The first hypothesis proposed for solving the puzzle postulates the existence of partially unfolded intermediates on the folding pathway, because partially unfolded intermediates allow the conformation space to be searched in a stepwise manner and very effectively reduce the time needed to reach the native state (*2*). From the late 1960s to the middle of the 1990s, most protein folding studies have been devoted to identifying and characterizing folding intermediates using various approaches (*3*). Indeed, partially unfolded intermediates have been identified and characterized for many proteins. Typical examples are apomyoglobin (*4*), hen egg white lysozyme (*5*), and ribonuclease H (*6*).

These proteins, however, are relatively large (>120 amino acids). Recent studies on smaller proteins (<120 amino acids) show that partially unfolded intermediates are usually not detectable in kinetic folding experiments (*7*, *8*). Therefore, doubts have been cast on the importance of folding intermediates in solving the Levinthal paradox for small proteins, and other models have been proposed or revived in recent years. For example, the nucleation (*9*) and jigsaw puzzle models (*10*) enriched with more physical and structural details have been used to describe the folding of small proteins (*11*−*14*). In particular, computer simulation studies on protein folding using lattice models have suggested that multiple structures in the transition state are important for solving the Levinthal paradox (*12*). Moreover, it has been suggested that the intermediates observed in the folding experiments are misfolded and serve as kinetic traps that impede the folding process instead of helping to search the conformational space (*13*, *14*).

The failure to observe intermediates in kinetic folding experiments alone, however, does not necessarily mean that they are absent, because certain rules prohibit intermediates from being observed in traditional kinetic studies (*15*). For an intermediate to become detectable, it must occupy a free energy well that is lower than all prior wells and must encounter a barrier that is higher (trough to peak) than all prior barriers (Figure 1A). When the later barrier for an intermediate to fold forward is smaller than the initial barrier of its formation (Type I, Figure 1B), or the intermediate is less stable than the unfolded state (Type II, Figure 1C), the intermediate cannot be observed in kinetic folding experiments. Here, we call these kinetically unobservable intermediates *hidden intermediates*. Type I hidden intermediates may be observed in kinetic unfolding or equilibrium experi-

* Corresponding author. Tel: 301-594-2375. Fax: 301-402-3095. E-mail: yawen@helix.nih.gov.

10.1021/bi0362267
Published on Web 03/02/2004

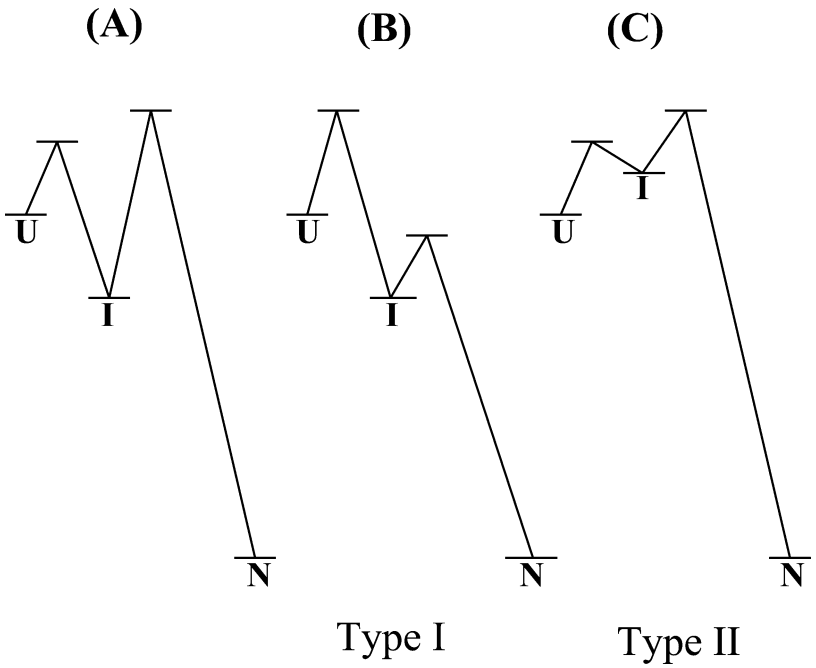

FIGURE 1: Free energy diagram illustration on the rules for observing folding intermediates using conventional ensemble kinetic methods. (A) Kinetically observable intermediate. The intermediate is more stable than the unfolded state. The kinetic barrier from the intermediate to the native state is higher than that from the unfolded state to the intermediate. (B) Type I hidden intermediate. The intermediate is more stable than the unfolded state. The kinetic barrier from the intermediate to the native state is smaller than that from the unfolded state to the intermediate state. (C) Type II hidden intermediate. The intermediate is less stable than the unfolded state. It is not directly detectable by either kinetic or thermodynamics methods.

ments. On the other hand, Type II hidden intermediate can only be observed indirectly with currently available experimental tools.

Previous studies on the folding pathway of barnase have encountered difficulties in defining both the rate-limiting transition state (TS_1)[1] at zero denaturant and a proposed hidden intermediate (I_2) that lies between TS_1 and the rate-limiting transition state (TS_2) at high denaturant concentrations (*16*−*18*). While TS_2 is well defined, with Φ values of ~1.0 at many positions, TS_1 has small ϕ values throughout the structure of the protein, in the absence of detectable early folding intermediates that are more stable than the unfolded state (*16*, *17*). Although this result appears to be consistent with the multipathway view of protein folding (Figure 2A), the mutations are those from larger hydrophobic residues to slightly smaller ones. Therefore, the small Φ values in TS_1 mainly reflect the lack of significant side chain−side chain interactions in the rate-limiting transition state. They provide no information for the secondary structure formation. It is still possible that most of the molecules fold through a defined transition state with the formation of specific secondary structure in which all of the side chains are significantly exposed (*17*) (Figure 2B). To distinguish the two possibilities, here we performed Gly scanning mutations at multiple positions in the structure of barnase and studied their effects on the folding rate. Since the Gly residue has a low propensity to form both α-helix and β-sheet, the Gly mutations can destabilize α-helix and β-sheet structures and provide probes for studying secondary structure formation in the rate-limiting transition state. Using this method, formation of secondary structures at a specific region of the native structure was identified.

For the hidden intermediate I_2, evidence for its existence is indirect. It is based on the nonlinear behavior of the logarithm of the unfolding rate constants k_u as a function of denaturant concentrations. Neither the stability nor the structure of the proposed intermediate is known. To see whether I_2 may be detected by native-state hydrogen exchange method, we performed the native-state hydrogen exchange experiment at pD_{read} 5 and 25 °C. This condition ensures that hydrogen exchange occurs in an EX2 mechanism under sufficiently low denaturant concentrations and allows intermediates that are more stable than the unfolded state to be detected. Although we failed to identify I_2, a new partially unfolded hidden intermediate (I_3) that exists after TS_2 was identified.

MATERIALS AND METHODS

Protein Mutation, Expression, and Purification. The studies presented in this paper used a pseudo-wild type (p-WT) of barnase, in which a surface residue in the active site H102 is mutated to Ala. This mutation abolished the enzymatic activity of barnase but had no effect on the structure of the protein as judged by the similar ^1H-^{15}N HSQC spectrum to the wild-type protein. p-WT can be expressed in *Escherichia coli* conveniently in the absence of coexpression of a barnase inhibitor. All mutants presented in this paper were made using a quick-change mutation kit (Stratgen, CA). Protein purification is as described before (*19*).

Kinetic Folding and Unfolding Experiments. Kinetic folding and unfolding experiments were done at pH 6.3 and

[1] Abbreviations: GdmCl, guanidinium chloride; HX, hydrogen exchange; TS, transition state.

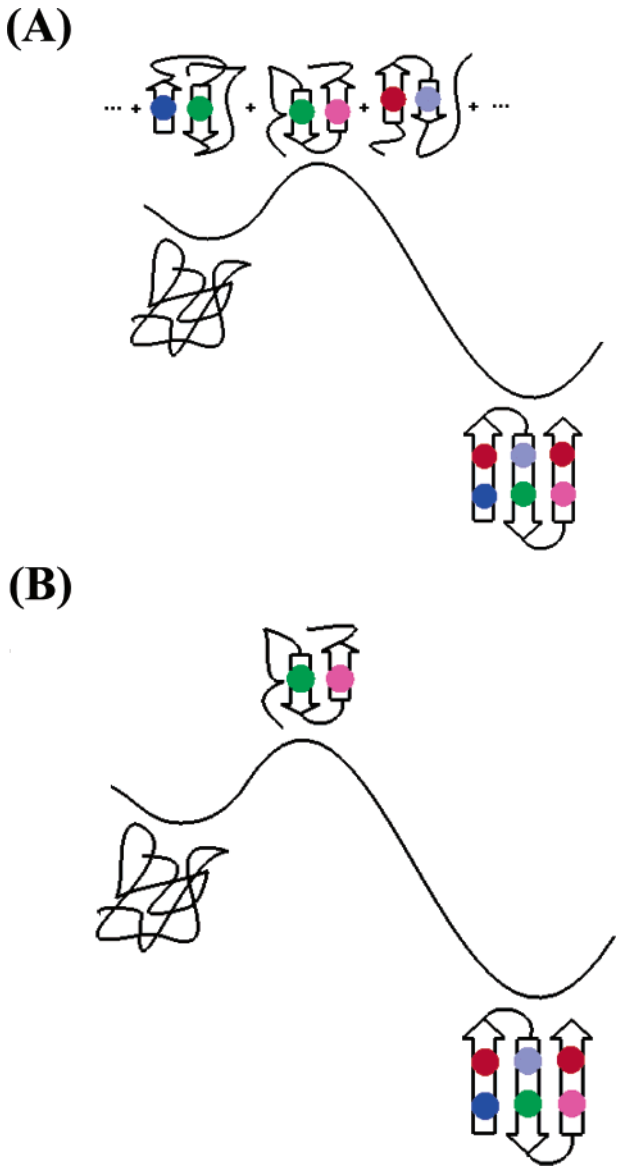

FIGURE 2: Illustration of the two different interpretations on the low ϕ values of the rate-limiting transition state of barnase under native conditions (*17*). (A) Multiple folding pathways. The folding rate is limited by the formation of nuclei with similar stability at multiple positions of the molecule. If a mutation destabilizes one of the nuclei, folding can still proceed through other nuclei without changing the folding rate significantly. (B) A single defined structure in the absence of full side chain interactions. Although the partially unfolded structure of the transition state is well defined, none of the mutations will have large ϕ values because all side chains are partially exposed. The colored solid circles represent side chains. Possible folding intermediates that exist after the rate-limiting transition state of barnase are not presented in the diagrams (see discussions in refs *16* and *17*).

25 °C, using a fast-mixing apparatus (Biologic, France) (*20*). In the kinetic folding experiments, a pH jump from 1.8 to pH 6.3 was used to initiate folding at different final concentrations of guanidinium chloride (GdmCl). Only the folding rate constant for the fast detectable kinetic phase was measured because the slow phases were known to be due to proline isomerization (*21*). Unfolding was initiated by diluting the folded proteins in the solution with high concentrations of GdmCl. The kinetic curve was fitted with a single exponential and a linear baseline using the equation: $I(t) = a(1 - \exp(-k_f t)) + bt + c$, where a, b, c, and k_f are floating parameters. k_f is the folding rate constant. $I(t)$ is the fluorescence signal at time t. The following equations were used to fit the measured folding and unfolding rate constants as a function of GdmCl concentrations:

$$k_{obs} = k_f + k_u \quad (2)$$

$$\log k_f = \log k_f^\circ + m_f\,[\mathrm{GdmCl}] \quad (3)$$

$$\log k_u = \log k_u^\circ + m_u\,[\mathrm{GdmCl}] \quad (4)$$

Thermal Melting of Barnase Mutants. Equilibrium melting monitored by CD at wavelength 230 nm was used to measure the stability of barnase mutants. The experiment was done at pH 6.3 (50 mM Mes). The melting curves were fitted with eq 5 using a fixed ΔC_p of 1.7 kcal/mol/deg (*22*).

$$\theta = \theta_u + (\theta_f - \theta_u)/\{1 + \exp[(-\Delta H_m/R)(1/T - 1/T_m) + (\Delta C_p/R)(((T_m/T) - 1) + \ln(T/T_m))]\} \quad (5)$$

Here, θ is the measured CD signal, θ_f and θ_u are linear functions of temperature representing the folded and unfolded baselines respectively (*23*). T_m is the melting temperature, and ΔH_m is the enthalpy of unfolding at T_m. Equation 6 is used to calculate the unfolding free energy.

$$\Delta G_{NU} = \Delta H_m(T - T_m) - \Delta C_p \ln(T/T_m) \quad (6)$$

Calculation of Φ_f and Φ_f^{sec} Values. Φ_f is defined as the ratio of the change in free energy of the transition state over that in the native state upon a single mutation (*24*). It is calculated using $-RT \ln(k_f^{mut}/k_f^{p-wt})/\Delta\Delta G_{NU}$. Φ_f^{sec} is defined as the ratio of the change in free energy in the transition state over the change in free energy due to formation of the secondary structure alone upon a single mutation. It is calculated using $-RT \ln(k_f^{mut}/k_f^{p-wt})/\Delta\Delta G$(propensity for secondary structure formation). In the case of the α-helix, 0.8 kcal/mol of $\Delta\Delta G$(α-helix propensity) for Ala to Gly mutation was used in the calculation. In the case of the β-sheet, the $\Delta\Delta G$(β-sheet propensity) values from the results of Minor and Kim (*23*) for β-sheet propensities were used. These values in the unit of kcal/mol are Ile, 2.2; Leu, 1.71; Val, 2.02; Glu, 1.21; Arg, 1.65; Thr, 2.3; Tyr, 2.16.

Theory of Native-State Hydrogen Exchange. Exchangeable amide hydrogens (NH) involved in the hydrogen-bonded structure can exchange with solvent hydrogens only when they are transiently exposed to solvent in some kind of closed-to-open reaction (*25*), as indicated in eq 7. Here, k_{op} is the kinetic opening rate constant, and k_{cl} is the kinetic closing rate constant equilibrium. k_{int} is the intrinsic exchange rate constants in the open form, which is normally derived from unfolded peptide models (*26*).

$$\mathrm{NH(closed)} \underset{k_{cl}}{\overset{k_{op}}{\rightleftarrows}} \mathrm{NH(open)} \xrightarrow{k_{int}} \mathrm{exchanged}; \qquad K_{op} = k_{op}/k_{cl} \quad (7)$$

When the closing reaction is faster than k_{int} (EX2 condition), the exchange rate of any hydrogen, k_{ex}, is determined by its chemical exchange rate in the open form multiplied by the equilibrium opening constant, K_{op}.

$$k_{ex} = K_{op} k_{int} \quad (8)$$

This leads to free energy for the dominant opening reaction:

$$\Delta G_{HX} = -RT \ln K_{op} = -RT \ln(k_{ex}/k_{int}) \quad (9)$$

where R is the gas constant and T is the temperature. The free energy of the hydrogen exchange as defined in eq 9, ΔG_{HX}, represents a combination of opening transitions from the EX2 mechanism, both structural unfolding and local fluctuations. Evaluating ΔG_{HX} as a function of denaturant [GdmCl] allows one to distinguish and separate these two processes. The addition of GdmCl promotes the population of partially unfolded and fully unfolded forms, since these states have more surface exposure than the native state, but by definition have no effect on the local structure fluctuations (*27*). By examining the pattern of ΔG_{HX} versus [GdmCl] of the amide proteins, one can obtain the structural and energetic information of the partially unfolded forms and fully unfolded state.

When the closing reaction is slower than k_{int} (EX1 condition), the exchange rate, k_{ex}, is determined by opening rate constant k_{op}. For the amide protons that can only exchange through global unfolding, the k_{op} will be the global unfolding rate constants.

Hydrogen Exchange Experiments. The hydrogen exchange experiments were initiated by loading a 0.5-mL protein sample in H_2O at pH 5.0 (20 mM NaAc) to a spin column (Sephdex 25, bed volume 3 mL) that was preequilibrated with D_2O at pD_{read} 5.0 (20 mM D_4-NaAc) at various concentrations of deuterated GdmCl for buffer exchange. The column was spun for 1 min at 4000 rpm using a benchtop centrifuge. The eluted protein sample was immediately transferred into an NMR tube for collecting a series of ^1H-^{15}N HSQC spectra. The concentrations of the protein samples were ~1 to 2 mM. The NMR spectra were processed using NMRPipe (*28*) and analyzed using NMRView (*29*) to obtain the exchange rate constants.

NMR Characterization of Intermediates. NMR spectra were collected at 25 °C and pH 6.3 on a Bruker (Bellerica, MA) DRX 500-MHz spectrometer equipped with a 5-mm x, y, z-shielded pulse field gradient triple resonance probe. HNCACB (*30*) and CBCACONH (*31*) were used to assign the backbone resonances. Steady-state ^1H-^{15}N dynamics NOE values were measured by recording ^1H-^{15}N HSQC spectra in the presence (NOE) and absence (NONOE) of ^1H saturation for 3 s (*32*). NOE and NONOE experiments were interleaved in one experiment to minimize the effect of uncertainty of the instrument. NMR spectra were processed using NMRPipe (*28*) and analyzed using NMRView (*29*). NOE is defined as the ratio of the cross-peak intensity with ^1H saturation over that without ^1H saturation in the ^1H-^{15}N HSQC spectra.

RESULTS

Effect of Ala versus Gly Mutations in α-Helix on the Folding Rate. In barnase, residues from 6 to 19 in the N-terminus form an α-helix, α_1 (see Figure 3). Earlier studies on the factors that affect the stability of α-helix have shown that different residues have different intrinsic propensities for the α-helix formation (*33*−*35*). In general, however, the differences are relatively small. The largest one is between Ala and Gly, which is ~0.8 kcal/mol. Therefore, in previous studies on the formation of α-helix in the rate-limiting transition state, mutations from Ala to Gly have been used to measure ϕ values (*36*). Here, we took a similar approach. Residues at positions 8, 12, 13, 15, and 17 were first mutated to Ala (Figure 3). Then, Ala was mutated to Gly. If the N-terminal helix were fully formed in the transition state, the mutation from Ala to Gly due to the intrinsic propensity alone would cause a decrease of the folding rate by a factor of 4 to yield the ~0.8 kcal/mol change in free energy. Folding rate constants were measured using stopped-flow fluorescence (*21*). The stability of the mutants was measured using temperature melting and monitored by CD signal at the wavelength 230 nm. For all of the chosen positions, no mutation has caused a significant change in the folding rate (see Table 1). The largest change in the folding rate is at position 17, which is less than a factor of 2. Therefore, these results indicate that the N-terminal helix cannot be dominantly formed in the transition state ensemble.

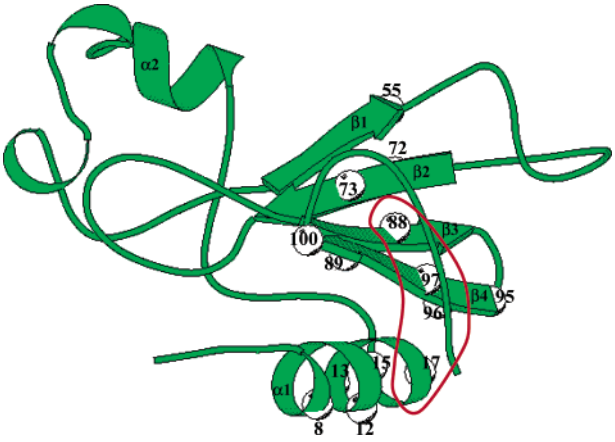

FIGURE 3: Structure of barnase and the positions for Gly mutations. The C_α carbons for the residues to be mutated are shown in balls. There are two Gly residues (52 and 53) in β1. Therefore, further mutations were not made in this region. The red curve illustrates the region that has large ϕ_f^{sec}. The structure is made using Molscript (*56*).

Effect of Gly Mutations in the β-Sheet on the Folding Rate. Next, we investigated the formation of the β-sheet in the transition state. In this case, it has been shown that the propensity of each residue toward β-sheet formation can be very different (*23*). For example, residues such as Ile, Val, and Thr have much higher propensities to form a β-sheet than Gly (*23*). The propensity difference between Ile and Gly reaches to 2.2 kcal/mol. The large differences in forming β-sheet structures for many residues relative to Gly indicate that the mutations from these residues to Gly would have a significant effect on the folding rate due to their propensities alone if the formation of the β-sheet structure dominated the transition state ensemble. Therefore, to investigate the β-sheet formation in the rate-limiting transition state, mutations to Glys were made directly from the residues with large β-sheet propensities. Eight Gly mutations that essentially covered all β-sheet regions of the protein were made individually (see Figure 3). Again, the kinetic folding rate and stability of the mutants were measured by stopped-flow fluorescence and temperature melting, respectively. We found that most of the mutations did not affect folding rates significantly except for I96G, Y97G, and I88G (see Table 1). In particular, I96G and Y97G mutations decreased the folding rates by 50- and 20-fold, respectively. Figure 4 illustrates the

Table 1: Thermodynamic and Kinetic Parameters for Barnase Mutants at pH 6.3 and 25 °C in 50 mM Mes

	T_m (K)	ΔH_m (kcal/mol)	k_f (s^{-1})	ΔG_{NU} (kcal/mol)	$\Delta\Delta G_{NU}$ (kcal/mol)	Φ_f
WT[a]	327.6	141.4	12.0	10.5		
p-WT	325.4	137.2	11.0	9.5		
α-helix						
D8G[a]	324.6	137.6	9.6	9.5	1.0	0.1
D8A[a]	325.6	140.1	9.6	9.9	0.6	0.2
D12G	323.1	128.7	9.4	8.3	1.2	0.1
D12A	324.4	152.8	11.6	10.6	−1.1	0.0
Y13G	309.8	92.7	5.9	3.1	6.4	0.2
Y13A[a]			7.2		3.7	0.1
Q15G	323.4	123.0	7.9	7.9	1.4	0.1
Q15A	324.5	136.7	11.9	9.3	0.2	0.2
Y17G	315.1	117.4	3.7	5.6	4.9	0.1
Y17A[a]	322.5	133.1	6.9	8.6	1.9	0.2
β-sheet						
I55G	320.1	111.7	9.6	6.4	3.1	0.0
R72G	319.7	122.8	8.4	7.0	2.5	0.0
E73G	312.7	100.6	8.8	4.1	5.4	0.1
I88G	304.6	100.4	**1.7**	2.1	7.4	0.2
L89G	316.7	58.5	13.1	2.5	7.0	0.0
L95G	316.3	98.5	4.5	4.8	4.7	0.1
I96G	309.7	110.3	**0.2**	3.8	5.7	0.4
Y97G	307.5	102.6	**0.5**	2.9	6.6	0.3
T100G	321.1	113.1	6.5	6.7	2.8	0.1

[a] Mutations based on the wild-type barnase are Y13A (*54*), Y17A (*54*), D8G (*55*), D8A (*55*). The folding rate constants reported here are for the fast kinetic phase in the absence of proline isomerization (*21*).

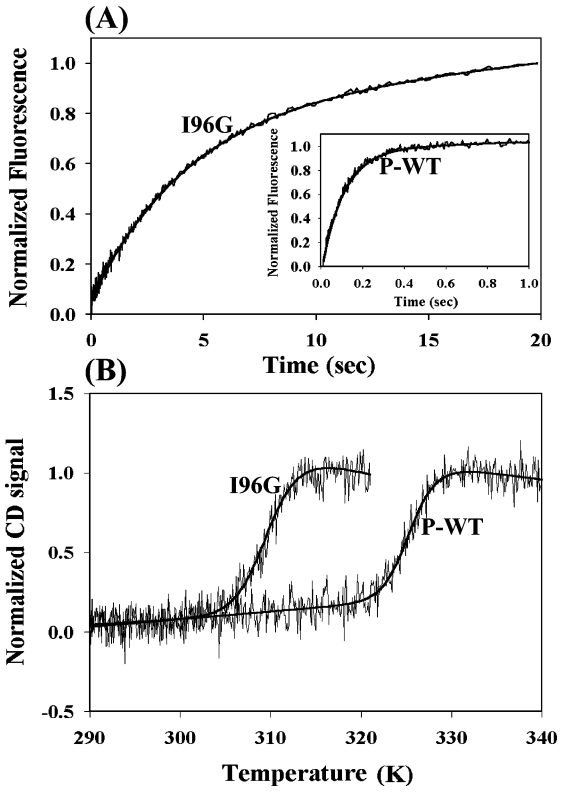

FIGURE 4: Representative kinetic traces and equilibrium melting curves for Gly mutants. (A) Kinetic traces of I96G and the p-WT (inset). (B) Equilibrium melting curves of I96G mutant and p-WT. All other mutants show similar melting curves, except that their T_m's are different.

experimental data for mutant I96G. The calculated Φ_f and Φ_f^{sec} are shown in Figure 5 (see methods for definitions of Φ_f and Φ_f^{sec}).

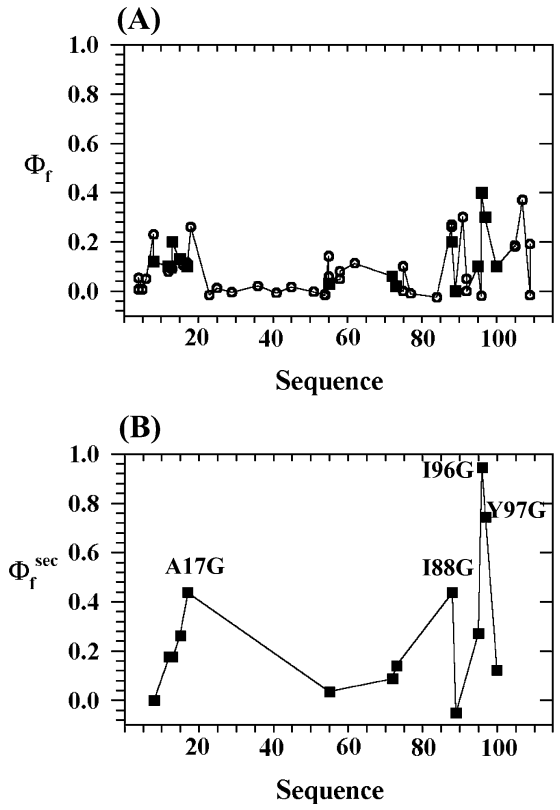

FIGURE 5: Distribution of ϕ_f and ϕ_f^{sec} values as a function of sequence. (A) The ϕ_f value distribution. Open circles are from earlier work (*17*, *54*). Filled squares are from this study. (B) ϕ_f^{sec} distribution.

Detection of Partial Unfolding by Native-State Hydrogen Exchange. Figure 6A shows the native-state hydrogen exchange results for typical amide protons that can be measured at pD_{read} 5.0 and 25 °C in D_2O (see methods). The ΔG_{HX}'s of amide protons V10 and N77 show denaturant-dependent behavior at low [GdmCl]. In contrast, W94 has the same ΔG_{HX} as V10 and N77 at zero denaturant but is independent of denaturant concentrations until it reaches to the global unfolding. In Figure 6A, a diverging behavior of ΔG_{HX}'s of N77 and W94 is clearly observable as denaturant concentration is increased. All other amide protons with measurable exchange rates have ΔG_{HX}'s independent of denaturant concentrations below 0.7 M GdmCl. Under these conditions, the folding rate is above 1 s^{-1}. The intrinsic exchange rate constants for these amide protons are all below 0.2 s^{-1}, indicating that the exchange occurs under EX2 mechanism. The slope of the ΔG_{HX} versus [GdmCl] below 0.7 M for amide protons of N77 and V10 is ∼0.9 kcal/mol, suggesting that a partial unfolding with significant exposure of surface area has occurred, in which the amide protons of V10 and N77 can dominantly exchange with solvent protons.

In the earlier hydrogen exchange experiment on barnase, it has been shown that 13 amino protons can exchange only in the fully unfolded state through global unfolding (*37*). These amide protons are shown in Figure 6B. The result indicates that the regions with the major α-helix and the β-sheet cannot be unfolded in any partially unfolded states that are more stable than the unfolded state. Therefore, any partial unfolding could only involve the loop regions in the barnase structure. There are two major loop regions as illustrated in Figure 6B. One is from residues 76 to 86

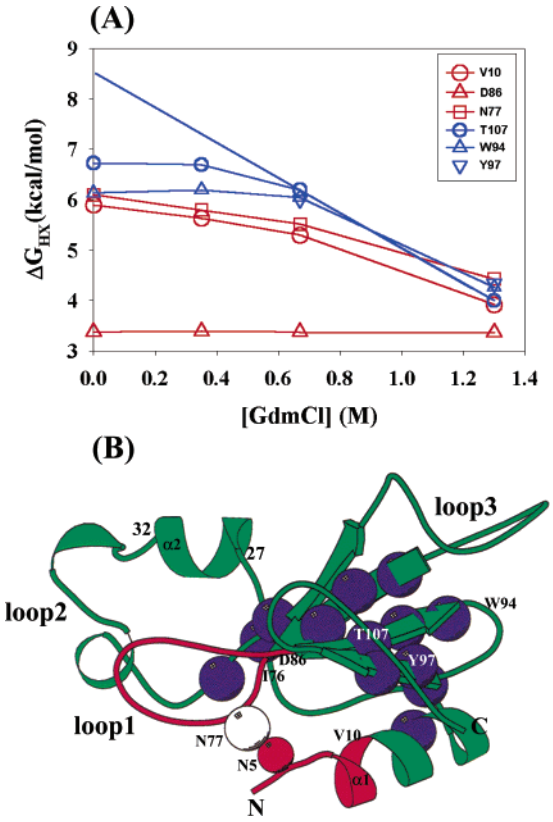

FIGURE 6: Native-state hydrogen exchange results at pD 5.0 and 25 °C. (A) Native-state hydrogen exchange results for typical amide protons. The spread of ΔG_{HX} values at 1.3 M GdmCl is due to the switch of hydrogen exchange mechanism since the folding rate is ~0.1 s^{-1}, which is close to the intrinsic exchange rate of N77. (B) Structure of barnase. The blue balls represent the amide protons that can only exchange through global unfolding (*37*). The red and white balls represent the oxygen atom of the side chain N77 and backbone hydrogen atom of N5, respectively. They form a hydrogen bond.

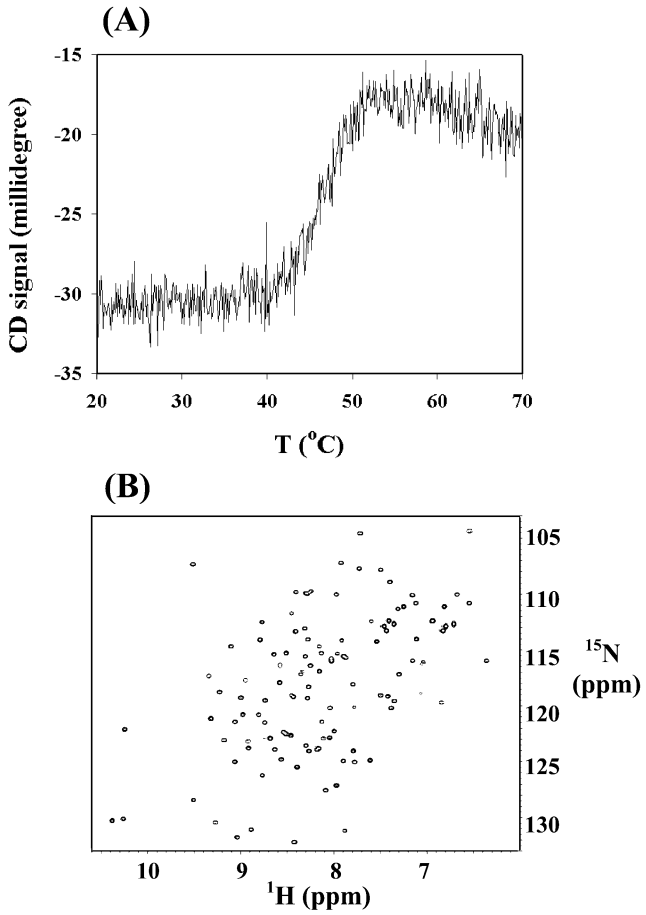

FIGURE 7: Stability of p-WT-5G (Y78G/F82G/R83G/N84G/N77G). (A) Melting curve of p-WT-5G observed at 230 nm. (B) ^{1}H-^{15}N HSQC spectrum of the mutant p-WT-5G at 25 °C.

(loop1). The other loop (loop2) is the region from residues 24 to 42, including a one-turn α-helix (α_2) from residues 27 to 31. It is also known that some amide protons in this loop have ΔG_{HX}'s larger than V10 and N77 (*38*), indicating that this region does not unfold together with residues N77 and V10, even though the hydrophobic residues in the two loops pack together to form a hydrophobic core. This leads to the possibility that loop1 might unfold independently as a cooperative unit, which is consistent with the fact that all of the amide protons in the omega loop from residues N77 to D86 have ΔG_{HX} values smaller than that of N77. Moreover, the backbone NH group of residue N77 forms a hydrogen bond with the backbone CO of residue N5. Unfolding of the loop1 is likely coupled with the structural change in the N-terminal helix (see Figure 6B), which could explain why V10 has a similar exchange behavior as N77, since the amide hydrogen of V10 forms a hydrogen bond with the backbone oxygen of residue 6.

Characterizing the Hidden Intermediate by Protein Engineering and NMR. The above native-state hydrogen exchange results are consistent with the unfolding of the omega loop from residues 77 to 86. However, they are insufficient to make definitive conclusion since only the ΔG_{HX} of amide proton, N77, is denaturant-dependent at low denaturant concentrations. To test whether the omega loop can unfold independently, we used Gly residues to substitute for the five important residues (Y78G/F82G/R83G/N84G/N77G) that form hydrophobic or hydrogen bonding or salt bridge interactions with other residues in the native structure. Suppose that the omega loop unfolds independently as a structural unit; these mutations would destabilize the native state but not the partially unfolded intermediate that has the omega loop unfolded. Therefore, this p-WT-5G mutant would be a mimic of the folding intermediate with the omega loop unfolded (*39*). Indeed, we found that the mutant is stable. It has a melting temperature of ~47 °C at pH 6.3 (Figure 7A).

We further characterized the structure of the mutant using multidimensional NMR. Figure 7B illustrates the ^{1}H-^{15}N HSQC spectrum of the mutant. The cross-peaks are well dispersed, suggesting that the protein is well folded. The resonance of ^{1}H, ^{15}N, and $^{13}C_{\alpha}$ has been assigned using triple resonance NMR methods. The C_{α} chemical shift data (Figure 8A) indicates that only loop1 and the residues at the N-terminal end of α1 have contiguous values close to those of random coil, suggesting that these regions can indeed unfold independently. This conclusion is further confirmed by the backbone ^{15}N dynamics studies. The dynamics NOEs data showed that the loop1 region and the residues from 1 to 6 have smaller NOEs values (Figure 8B), suggesting that they are more mobile and presumably unfolded. It should be noted that the mutations also have effects on a small loop from residues 100 to 105 (see Figure 3) that are close to loop 1. The ^{1}H-^{15}N cross-peaks in this region are missing in

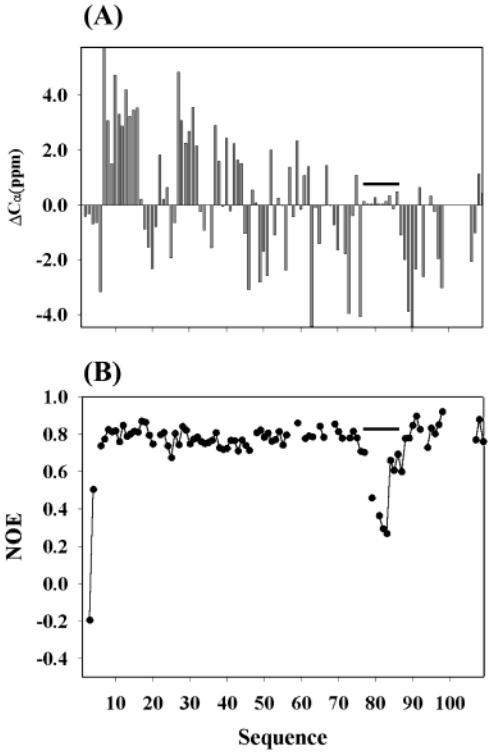

FIGURE 8: Structural characterization of p-WT-5G. (A) The difference of C_α chemical shifts between the p-WT-5G and random coil (*57*), and (B) ^{1}H-^{15}N NOEs of the p-WT-5G mutant. The thick black lines indicate the region from residue 76 to 86.

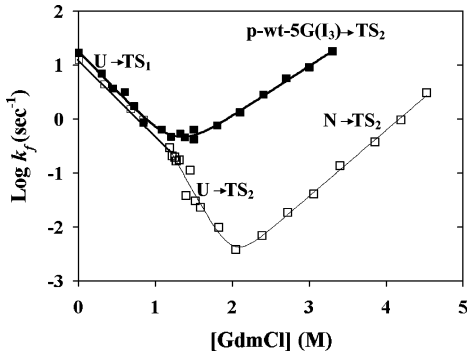

FIGURE 9: Chevron plot of p-WT-5G mutant and the wild-type barnase. For the fitting parameters, please see Table 2. The global unfolding of p-WT-5G coincides with the switch between TS_1 and TS_2. Therefore, a curved folding arm in the chevron plot is not observed.

the ^{1}H-^{15}N HSQC spectra at 25 °C, indicating that there is a conformational exchange on the millisecond time scale. These peaks, however, could be observed at lower temperature such as 10 °C.

Kinetic Folding and Unfolding of p-WT-5G. To see how p-WT-5G, the mimic of the hidden folding intermediate, folds and unfolds kinetically, we measured its folding and unfolding rate constants as a function of denaturant concentrations. Figure 9 shows the logarithm of the observed folding/unfolding rate constants for the major kinetic phase as a function of [GdmCl]. The folding rate and its dependence on the denaturant concentration are very similar to the wild-type protein. In contrast, the unfolding rate constant is much larger and becomes less dependent on the concentrations of denaturant than that of wild-type protein.

DISCUSSIONS

The Rate-Limiting Transition State and the Unfolded State Ensemble Under Native Conditions. Glycine scanning mutation studies show that most of the positions have little effect on the folding rate except those at positions 96, 97, and 88. I96G, Y97G, and I88G have changed the folding rates by 50-, 20-, and 6-fold, respectively, indicating that they have increased the activation free energy by 2.3, 1.8, and 1.2 kcal/mol, respectively. These results suggest that some specific structures or interactions involving these residues have formed in the rate-limiting transition state. However, these mutations have decreased the stability of the native state more than what they do for the transition state (see Table 1); therefore, the interactions formed in the transition state among these residues are much weaker than those in the native state. To observe such partial interactions by the mutation effect on folding rates, it requires that any sub-millisecond intermediates that have the region including residues I96 and Y97 folded either have much less interactions among these residues or are not significantly more stable than the unfolded state. This result is consistent with the earlier conclusion from the hydrogen exchange experiments that there are no stable secondary structures populated in the sub-millisecond time scale of the folding.

Interestingly, if one assumes that the mutation effect on the folding rate is solely caused by the propensity for formation of secondary structures, near 1.0 values of ϕ_f^{sec} (see methods) were obtained for residues I96 and Y97. Moreover, all residues that have larger ϕ_f^{sec} values are clustered in the same region of the structure (see Figure 3), suggesting that the formation of secondary structures in this region is the rate-limiting step. Thus, even though barnase has unusual small ϕ values throughout the structure, the Gly scanning mutation studies indicate that the folding behavior of barnase is still consistent with the existence of defined structures in the transition state rather than numerous different structures with similar free energy.

Hidden Intermediates on the Folding Pathway of Barnase. Previously, the structure of the rate-limiting transition state of barnase under denaturing conditions (TS_2) has been characterized using the Φ-value analysis (*40*). It shows that major secondary structures are formed but the loops are unfolded. Thus, p-WT-5G is more folded than TS_2, suggesting it exists after TS_2 on the folding pathway. Consequently, p-WT-5G is not the proposed hidden intermediate I_2 in the earlier studies (*16*). Here, we named the intermediate detected by the native-state hydrogen exchange and mimicked by p-WT-5G as I_3. The placement of I_3 after TS_2 is consistent with the kinetic folding and unfolding results (Figure 9). p-WT-5G folded with the same rate and denaturant dependence as the wild-type protein. The sum of m_f and m_u for p-WT-5G is significantly smaller (by 1.9 kcal/mol) than the global equilibrium unfolding m_{NU} value of the wild-type protein (see Figure 9 and Table 2), indicating that the switch of transition states from TS_1 to TS_2 also occurred to p-WT-5G as denaturant concentrations increased. It should be noted that the global unfolding transition occurred concurrently with the switch of transition states for p-WT-5G (Figure 9). Therefore, a curved folding arm in the chevron plot is not observed.

Table 2: Kinetic Parameters for the Folding and Unfolding of p-WT-5G and WT Barnase[a]

proteins	k_f^o U → TS_1	k_f^o U → TS_2	k_u^o N → TS_2	m_f U → TS_1	m_f U → TS_2	m_u N or I_3 → T
p-WT-5G	18.3		1.6×10^{-2}	2.01		1.26
WT	14.0	2.9×10^2	8.0×10^{-6}	2.01	3.47	1.66

[a] The units for rate constant and m-values are s^{-1} and kcal/mol/[GdmCl](M), respectively. The equilibrium global unfolding m_{NU} for wild-type protein is $m_f(U \rightarrow TS_2) + m_u(N \rightarrow TS_2) = 5.13$ kcal/mol/M.

Regarding this new hidden intermediate, it should be noted that the log k_u of wild-type barnase versus denaturant concentrations has been shown to deviate from linearity at high concentrations of urea (*41*). Matouschek et al. (*41*) have attributed this nonlinear behavior to the Hammond effect with a continuous movement of the transition state. Recently, Sanchez and Kiefhabor (*42*), however, have argued that the curvature in the unfolding arm of the chevron plot is due to the existence of a folding intermediate, which appears to be consistent with the results presented here.

The Sub-Millisecond State (D_{phys} or I_1) in the Folding of Barnase. The discussion on the folding pathway of barnase so far has assumed that no sub-millisecond intermediates that are more stable than the unfolded state exist. This is based on the recent H/D exchange results in the kinetic folding (*17*) and the reanalysis of the native-state hydrogen exchange data (*16*). Recently, Khan et al. (*18*) have studied the initial process of the refolding of denatured barnase and observed a small change of fluorescence signal in the sub-millisecond time scale. Accordingly, it is concluded that the sub-millisecond state is an intermediate state (I_1) or a denatured state under physiological conditions (D_{phys}). However, the thermodynamic stability of I_1 or D_{phys} is not determined. Available experimental data suggests that I_1 or D_{phy} is less stable than the fully unfolded random flying chain U. This is because I_1 has been assumed to involve the formation of some secondary structures in α_1 and α_2 that require the formation of hydrogen bonds for some amide protons (*18*). If I_1 is more stable than U, the amide hydrogens that form the hydrogen bonds in these secondary structures should exchange more slowly than the intrinsic exchange rates of nonstructured amide protons. This is, however, not observed in the hydrogen exchange folding competition experiment, even in the presence of stabilizing salt (0.4 M Na_2SO_4) (*17*).

The Kinetic Folding Pathway of Barnase. On the basis of the available experimental data, Figure 10 illustrates the simplest folding pathway of barnase. Under native conditions, the unfolded state ensemble contains a small fraction of I_1 or D_{phys}. It forms from the random flying chain U in the sub-millisecond time scale with a small change of fluorescence (*18*). The rate-limiting transition state is TS_1 and mainly involves the formation of a β-hairpin ($\beta_3-\beta_4$). The next observable rate-limiting transition state is TS_2 at higher denaturant concentrations (*40*). It is the switch between TS_1 and TS_2 as the rate-limiting transition state that causes the nonlinear behavior of the logarithm of the folding and unfolding rate constants at low denaturant concentrations (*43, 46*). Between TS_1 and TS_2, there could be one or more intermediates as represented by I_2 (*19, 43*). However, a smooth broad barrier between TS_1 and TS_2 cannot be excluded based on the available experimental data (*17, 44*). After TS_2, there is the hidden intermediate I_3 with the omega loop from residues 77 to 86 unfolded.

Native-State Hydrogen Exchange and Protein Folding Pathway of Barnase. It is useful to point out that after a few years' investigation on the relationship between native-state hydrogen exchange results and the folding pathway of barnase by both our and Fersht's groups, a consensus view has emerged. Mainly the stable sub-millisecond folding intermediate detected in the earlier $^1H/^2H$ pulse-labeling experiment and implied by the curved chevron plot is due to an aggregation artifact (*16, 19, 21, 45*). No sub-millisecond intermediates with significant protections for amide protons exist on the folding pathway of barnase (*16, 18, 46*). The curved folding arm in the chevron plot of barnase was due to the switch between TS_1 and TS_2 (*16, 17*). The earlier native-state hydrogen exchange experiment failed to identify any partially unfolded states because it was largely done under EX1 conditions at higher pD (6.8) and temperature (30 °C) (*38*). No hydrogen exchange results of barnase conflict with its kinetic folding pathway.

It is also useful to point out that Khan et al. (*18*) have stated that we disputed every existence of intermediates of barnase (*17*). This is a misunderstanding. Our view on protein folding has been that proteins in general fold through intermediates, although some of them may be hidden and are not detectable in traditional kinetic folding experiments (*15*). For the last several years, the focus of our research group has been to identify and characterize such hidden intermediates in small apparent two-state proteins (*47*). Recently, we have shown that Rd-apocyt b_{562}, a four-helix bundle protein, also folds through structured hidden intermediates (*39*). In this case, we have solved the high-resolution structure of one of the hidden intermediates (*48*). We now have provided the evidence for the existence of a new hidden intermediate (I_3) for barnase. In the case of I_2 for barnase, we do not feel that it has been proved beyond reasonable doubt as suggested by Khan et al. (*18*) because no information on the structure, stability, and kinetics of the proposed intermediate is known. Similarly, it is also useful to clarify that the Englander and Sosnick groups have only questioned the evidence for the "burst phase" intermediates (*8*) and not for distinct intermediates and pathways in general, which their work strongly supports (*49*). Hence, there is no disagreement between their position and the work of Sanchez and Kiefhaber on hidden intermediates (*50*), as implied in Khan et al. (*18*). Moreover, Khan et al. (*18*) placed no kinetic barrier between U and I_1 or D_{phy} in their free-energy diagram and suggested that the conversion between U and I_1 should be considered as a second-order rather than a first-order transition. This view by nature is not particularly different from the proposal of Sosnick et al. (*51*) that many "burst phase intermediates" are simply the unfolded states under native conditions, as called D_{phys} by Khan et al. (*18*).

Hidden Intermediates and the Levinthal Paradox. Many experimental studies of protein folding have focused on identifying and characterizing folding intermediates to demonstrate that partially unfolded intermediates are important to solve the large-scale conformational search problem, i.e., the Levinthal paradox (*2*). However, recent studies show that small proteins generally lack detectable intermediates in kinetic folding experiments. The work on barnase pre-

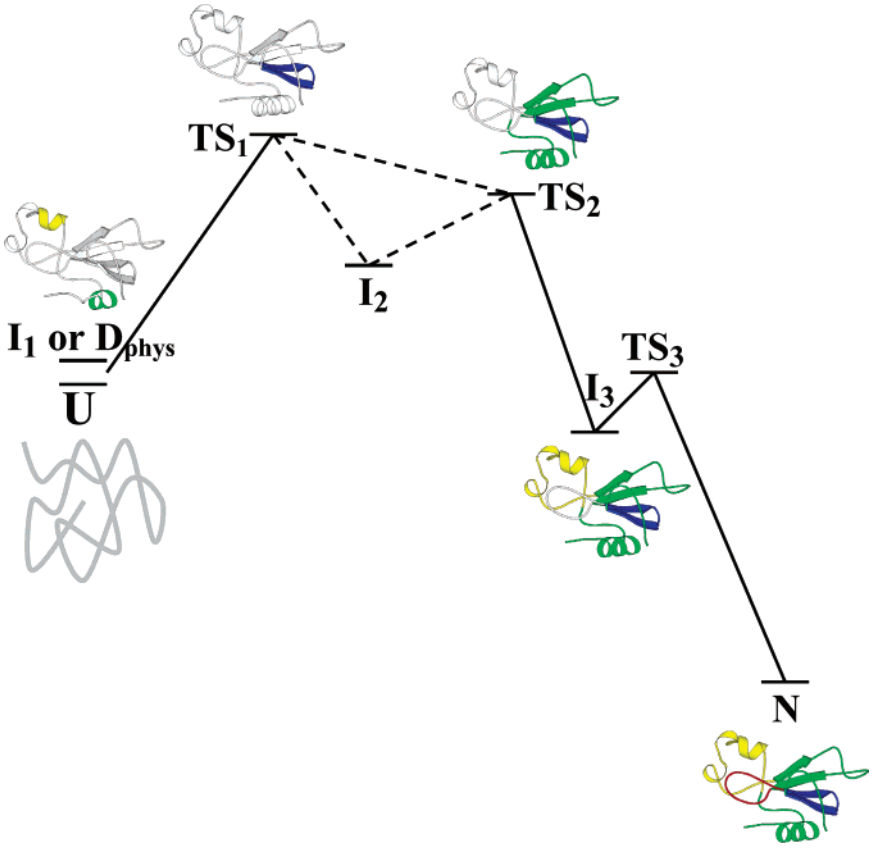

FIGURE 10: Free energy diagram illustration of the folding pathway of barnase under native conditions. Light gray represents unfolded regions. Colored regions represent folded regions. The structure of I_1 or D_{phys} is implied based on the studies of the acid denatured barnase, which showed C_α chemical shift deviated from random coil values in the region of α_1 and α_2 helices (*18*, *58*). It is not known whether I_1 is on- or off-pathway. It should be pointed out that the structures of the intermediates and transition states presented here are approximate illustrations of the available experimental data. By no means are the exact structures implied here.

sented here indicates that the partially unfolded intermediates can exist after the rate-limiting transition state, which is consistent with the earlier results from the studies on cyt *c* and Rd-apocyt b_{562}. Together, these results suggest that hidden intermediates may exist generally in small proteins.

It should be noted that the role of a partially unfolded intermediate in solving the Levinthal paradox should not be confused with its role in determining the folding rate (*13*). Whether an intermediate exists before or after the rate-limiting step does not change its role in solving the Levinthal paradox. For example, at pH 4.9, cyt *c* folds on a millisecond time scale through the partially unfolded intermediates that are after the rate-limiting step (*52*). At pH 6.2, folding of cyt *c* occurs on a time scale of seconds with the population of an early folding intermediate that has a misligation (*53*). In the latter case, the observed slow folding rate is controlled by the non-native covalent misligation in the intermediate. Although this misfolded intermediate may be considered as a kinetic trap due to its association with the slow folding rate and non-native interactions, it plays the same role as the late intermediate at pH 4.9 in solving the large-scale conformational search.

CONCLUSIONS

The experimental results reported here suggest that the folding pathway of barnase under native conditions involves the formation of secondary structures at a specific region in the rate-limiting transition state and a stable hidden intermediate with an omega loop unfolded under native conditions. Taking the previous experimental data on the folding pathway of barnase together, the folding pathway of barnase, although dominated with β-sheet structures, is similar to those of α-helical proteins: cyt *c* and Rd-apocyt b_{562}. All three proteins have partially unfolded intermediates after the rate-limiting step. These results suggest that other apparent two-state proteins may also fold through partially unfolded hidden intermediates.

ACKNOWLEDGMENT

We thank Mr. C. Do for protein purification and Drs. S. Walter Englander and Tobin R. Sosnick for their helpful comments.

REFERENCES

1. Levinthal, C. (1968) Are there pathways for protein folding? *J. Chem. Phys. 65*, 44−45.
2. Baldwin, R. L. (1997) The problem was to find the problem. *Protein Sci. 6*, 2031−2034.
3. Kim, P. S., and Baldwin, R. L. (1982) Intermediates in the folding reactions of small proteins. *Annu. Rev. Biochem. 59*, 631−660.
4. Hughson, F. M., Wright, P. E., and Baldwin, R. L. (1990) Structural characterization of a partly folded apomyoglobin intermediate. *Science 249*, 1544−1548.
5. Dobson, C. M. (1994) Understanding how proteins fold: the lysozyme story so far. *Trends Biochem. Sci. 19*, 31−37.
6. Chamberlain, A. K., Handel, T. M., and Marqusee, S. (1996) Detection of rare partially folded molecules in equilibrium with the native conformation of RNaseH. *Nat. Struct. Biol. 3*, 782−787.

7. Jackson, S. E. (1998) How do small single-domain proteins fold? *Folding Des. 3*, R81−R91.
8. Krantz, B. A., Mayne, L., Rumbley, J., Englander, S. W., and Sosnick, T. R. (2002) Fast and slow intermediate accumulation and the initial barrier mechanism in protein folding. *J. Mol. Biol. 324*, 1−13.
9. Wetlaufer, D. B. (1990) Nucleation in protein folding−confusion of structure and process. *Trends. Biochem. Sci. 15*, 414−415.
10. Harrison, S. C., and Durbin, R. (1985) Is there a single pathway for the folding of a polypeptide chain? *Proc. Natl. Acad. Sci. U.S.A. 82*, 4028−4030.
11. Itzhaki, L. S., Otzen, D. E., and Fersht, A. R. (1995) The structure of the transition state for folding of chymotrypsin inhibitor 2 analyzed by protein engineering methods: evidence for a nucleation-condensation mechanism for protein folding. *J. Mol. Biol. 254*, 260−288.
12. Sali, A., Shakhnovich, E., and Karplus, M. (1994) How does a protein fold? *Nature 369*, 248−251.
13. Wolynes, P. G., Onuchic, J. N., and Thirumalai, D. (1995) Navigating the folding routes. *Science 267*, 1619−1620.
14. Dill, K. A., and Chan, H. S. (1997) From Levinthal to pathways to funnels. *Nat. Struct. Biol. 4*, 10−19.
15. Bai, Y., and Englander, S. W. (1996) Future directions in folding: the multi-state nature of protein structure. *Proteins 24*, 145−151.
16. Fersht, A. R. (2000) A kinetically significant intermediate in the folding of barnase. *Proc. Natl. Acad. Sci. U.S.A. 97*, 14121−14126.
17. Chu, R. A., and Bai, Y. (2002) Lack of definable nucleation sites in the rate-limiting transition state of barnase under native conditions. *J. Mol. Biol. 315*, 761−772.
18. Khan, F., Chuang, J. I., Gianni, S., and Fersht, A. R. (2003) The kinetic pathway of folding of barnase. *J. Mol. Biol. 333*, 169−186.
19. Chu, R. A., Takei, J., Barchi, J. J., Jr., and Bai, Y. (1999) Relationship between the native-state hydrogen exchange and the folding pathways of barnase. *Biochemistry 38*, 14119−14124.
20. Chu, R. A., Takei, J., Barchi, J. J., Jr., and Bai, Y. (1999) Relationship between the native-state hydrogen exchange and the folding pathways of barnase. *Biochemistry 38*, 14119−14124.
21. Matouschek, A., Kellis, J. T., Jr., Serrano, L., Bycroft, M., and Fersht, A. R. (1990) Thransient folding intermediates characterized by protein engineering. *Nature 346*, 440−445.
22. Johnson, C. M., and Fersht, A. R. (1995) Protein stability as a function of denaturant concentration: the thermal stability of barnase in the presence of urea. *Biochemistry 34*, 6795−6804.
23. Minor, D. L., Jr., and Kim, P. S. (1994) Measurement of the beta-sheet-forming propensities of amino acids. *Nature 367*, 660−663.
24. Fersht, A. R., Matouschek, A., and Serrano, L. (1992) The folding of an enzyme I. Theory of protein engineering analysis of stability and pathway of protein folding. *J. Mol. Biol. 224*, 771−782.
25. Hvidt, A., and Nielsen, S. O. (1966) Hydrogen exchange in proteins. *Adv. Protein Chem. 21*, 287−386.
26. Bai, Y., Milne, J. S., Mayne, L., and Englander, S. W. (1993) Primary structure effects on peptide group hydrogen exchange. *Proteins 17*, 75−86.
27. Mayo, S. L., and Baldwin, R. L. (1993) Guanidinium chloride induction of partial unfolding in amide proton exchange in RNase A. *Science 262*, 873−876.
28. Delaglio, F., Grzesiek, S., Vuister, G., Zhu, G., Pfeifer, J., and Bax, A. (1995) NMRPipe: a multidimensional spectral processing system based on UNIX Pipes. *J. Biomol. NMR 6*, 277−293.
29. Johnson, B. A., and Blevins, R. A. (1994) NMRView: A computer program for the visualization and analysis of NMR data. *J. Biomol. NMR 4*, 603−614.
30. Wittekind, M., and Mueller, L. (1993) HNCACB, a high-sensitivity 3D NMR experiment to correlate amide proton and nitrogen resonaces with the alpha and beta carbon resonaces in proteins. *J. Magn. Reson. Ser. B 101*, 201−205.
31. Grzesiek, S., Ikura, M., Gronenborn, A. M., Clore, G. M., and Bax, A. (1992) An efficient experiment for sequential backbone assignment of medium sized isotopically enriched protiens. *J. Magn. Reson. 96*, 215−221.
32. Farrow, N. A., Muhandiram, R., Singer, A. U., Pascal, S. M., Kay, C. M., Gish, G., Shoelson, S. E., Pawson, T., Forman-Key, J. D., and Kay, L. E. (1994) Backbone dynamics of a free and a phosphopeptide-complexed src homolog domain studied by ^{15}N NMR relaxation. *Biochemistry 33*, 5984−6003.
33. Padmanabhan, S., Marqusee, S., Ridgeway, T., Laue, T. M., and Baldwin, R. L. (1990) Relative helix-forming tendencies of nonpolar amino acids. *Nature 344*, 268−270.
34. Lyu, P. C., Liff, M. I., Marry, L. A., and Kallenbach, N. R. (1990) Side chain contributions to the stability of alpha-helix structures in peptides. *Science 250*, 669−673.
35. O'Neil, K. T., and DeGrado, W. F. (1990) A thermodynamic scale for the helix-forming tendencies of the commonly occurring amino acids. *Science 250*, 646−651.
36. Burton, R. E., Huang, G. S., Daugherty, M. A., Calderone, T. L., and Oas, T. G. (1997) The energy landscape of a fast-folding protein mapped by Ala → Gly substitutions. *Nat. Struct. Biol. 4*, 305−310.
37. Clarke, J., Hounslow, A. M., Bycroft, M., and Fersht, A. R. (1993) Local breathing and global unfolding in hydrogen exchange of barnase and its relationship to protein folding pathways. *Proc. Natl. Acad. Sci. U.S.A. 90*, 9837−9841.
38. Clarke, J., and Fersht, A. R. (1996) An evaluation of the use of hydrogen exchange at equilibrium to probe intermediates on the protein folding pathway. *Folding Des. 1*, 243−254.
39. Chu, R. A., Pei, W. H., Takei, J., and Bai, Y. (2002) Relationship between the native-state hydrogen exchange and folding pathways of a four-helix bundle protein. *Biochemistry 41*, 7998−8003.
40. Serrano, L., Matouschek, A., and Fersht, A. R. (1992) The folding of an Enzyme III. Structure of the transition state for unfolding of barnase analysed by a protein engineering procedure. *J. Mol. Biol. 224*, 805−818.
41. Matouschek, A., Matthews, J. M., Johnson, C. M., and Fersht, A. R. (1994) Extrapolation to water of kinetic and equilibrium data for the unfolding of barnase in urea solutions. *Protein Eng. 7*, 1089−1095.
42. Sanchez, I. E., and Kiefhaber, T. (2003) Evidence for sequential barrier and obligatory intermediates in apparent two-state protein folding. *J. Mol. Biol. 325*, 367−376.
43. Fersht, A. R. (2000) A kinetically significant intermediate in the folding of barnase. *Proc. Natl. Acad. Sci. U.S.A. 97*, 14121−14126.
44. Kaya, H., and Chan, H. S. (2002) Toward a consistent modeling of protein thermodynamic and kinetic cooperativity: How applicable is the transition state picture to folding and unfolding? *J. Mol. Biol. 315*, 899−909.
45. Bycroft, M., Matouschek, A., Kellis, J. T., Serrano, L., and Fersht, A. R. (1990) Detection and characterization of a folding intermediate in barnase by NMR. *Nature 346*, 488−490.
46. Takei, J., Chu, R. A., and Bai, Y. (2000) Absence of stable intermediates on the folding pathway of barnase. *Proc. Natl. Acad. Sci. U.S.A. 97*, 10796−10801.
47. Bai, Y. (2003) Hidden intermediates and the Levinthal paradox in small proteins. *Biochem. Biophys. Res. Commun. 305*, 785−788.
48. Feng, H., Takei, J., Lipsitz, R., Tjandra, N., and Bai, Y. (2003) Specific non-native hydrophobic interactions in a hidden intermediate: Implications for protein folding. *Biochemistry 42*, 12461−12465.
49. Rumbley, J., Hoang, L., Mayne, L., and Englander, S. W. (2001) An amino acid code for protein folding. *Proc. Natl. Acad. Sci. U.S.A. 98*, 105−112.
50. Sanchez, I., and Kiefhaber, T. (2003) Evidence for sequential barriers and obligatory intermediates in apparent two-state protein folding. *J. Mol. Biol. 325*, 367−376.
51. Sosnick, T. R., Mayne, L., and Englander, S. W. (1996) Molecular collapse: the rate-limiting step in two-state cytochrome *c* folding. *Proteins 24*, 413−426.
52. Sosnick, T. R., Mayne, L., Hiller, R., and Englander, S. W. (1994) The barriers in protein folding. *Nat. Struct. Biol. 1*, 149−156.
53. Roder, H., Elove, G. A., and Englander, S. W. (1988) Structural characterization of folding intermediates in cytochrome *c* by H-exchange labeling and proton NMR. *Nature 335*, 700−704.
54. Matouschek, A., Serrano, L., and Fersht, A. R. (1992) The folding of an enzyme IV. Structure of an intermediate in the refolding of barnase analyzed by a protein engineering procedure. *J. Mol. Biol. 224*, 819−835.
55. Dalby, P. A., Oliveberg, M., and Fersht, A. R. (1998) Folding intermediates of wild-type and mutants of barnase. I. Use of phi-value analysis and m-values to probe the cooperative nature of the folding pre-equilibrium. *J. Mol. Biol. 276*, 625−646.

56. Kraulis, P. J. (1991) MOLSCRIPT: a program to produce both detailed and schematic plots of protein structures. *J. Appl. Crystallogr. 24*, 946−950.
57. Schwarzinger, S., Kroon, G. J. A., Foss, T. R., Chung, J., Wright, P. E., and Dyson, H. J. (2001) Sequence-dependent correction of random coil NMR chemical shifts. *J. Am. Chem. Soc. 123*, 2970−2978.
58. Arcus, V. L., Vuilleumier, S., Freund, S. M., Bycroft, M., and Fersht, A. R. (1995) A comparison of the pH, urea, and temperature-denatured states of barnase by heteronuclear NMR: implications for the initiation of protein folding. *J. Mol. Biol. 254*, 306−321.

BI0362267